Reliability analysis of InGaN/GaN multi-quantum-well solar cells under thermal stress

Xuanqi Huang, Houqiang Fu, Hong Chen, Zhijian Lu, Izak Baranowski, Jossue Montes, Tsung-Han Yang, Brendan P. Gunning, Dan Koleske, and Yuji Zhao

Citation: Appl. Phys. Lett. **111**, 233511 (2017);
View online: https://doi.org/10.1063/1.5006650
View Table of Contents: http://aip.scitation.org/toc/apl/111/23
Published by the American Institute of Physics

Reliability analysis of InGaN/GaN multi-quantum-well solar cells under thermal stress

Xuanqi Huang,[1] Houqiang Fu,[1] Hong Chen,[1] Zhijian Lu,[1] Izak Baranowski,[1] Jossue Montes,[1] Tsung-Han Yang,[1] Brendan P. Gunning,[2] Dan Koleske,[2] and Yuji Zhao[1,a)]
[1]*School of Electrical, Computer and Energy Engineering, Arizona State University, Tempe, Arizona 85287, USA*
[2]*Sandia National Laboratories, MS 0601, P.O. Box 5800, Albuquerque, New Mexico 87185-0601, USA*

(Received 26 September 2017; accepted 24 November 2017; published online 7 December 2017)

We investigate the thermal stability of InGaN solar cells under thermal stress at elevated temperatures from 400 °C to 500 °C. High Resolution X-Ray Diffraction analysis reveals that material quality of InGaN/GaN did not degrade after thermal stress. The external quantum efficiency characteristics of solar cells were well-maintained at all temperatures, which demonstrates the thermal robustness of InGaN materials. Analysis of current density–voltage (*J–V*) curves shows that the degradation of conversion efficiency of solar cells is mainly caused by the decrease in open-circuit voltage (V_{oc}), while short-circuit current (J_{sc}) and fill factor remain almost constant. The decrease in V_{oc} after thermal stress is attributed to the compromised metal contacts. Transmission line method results further confirmed that p-type contacts became Schottky-like after thermal stress. The Arrhenius model was employed to estimate the failure lifetime of InGaN solar cells at different temperatures. These results suggest that while InGaN solar cells have high thermal stability, the degradation in the metal contact could be the major limiting factor for these devices under high temperature operation. *Published by AIP Publishing.* https://doi.org/10.1063/1.5006650

III–nitride (III–N) material systems have attracted extensive research interest in both electronics and optoelectronics, including high-electron-mobility transistors,[1] power diodes,[2–4] solid-state lighting,[5–7] photovoltaics (PV),[8–11] photodetectors,[12–14] and visible light communication.[15] Due to their unique properties, such as tunable wide bandgaps,[16] high absorption coefficient, high thermal stability, and outstanding radiation resistance,[17] InGaN materials have also been proposed as ideal candidates for PV applications especially for high temperature operation or in a harsh environment. For example, InGaN solar cells have been proposed for applications in thermal (PVT) hybrid solar collector systems[18] and terrestrial concentrated PV systems[19] and for space explorations.[10] For next generation concentrated PVT hybrid systems, a higher operation temperature (>400 °C) due to higher concentrations is required when compared to conventional concentrated PV systems. For space missions near the Sun, the operating temperature of the PV systems can range from 450 °C for the Mercury mission[20] to 1400 °C for the Solar Probe mission.[21] Therefore, efficient and reliable operation of solar cells at high temperatures is critical for these applications, where III-N materials and devices hold great promise.[21,22]

By virtue of their large bandgaps and high atomic displacement energies,[23] III–N materials and devices are promising for high temperature applications. To date, high temperature operation of III–N devices has been theoretically predicted and experimentally demonstrated up to 600 °C in air and 1000 °C in vacuum.[24–28] For III-N InGaN solar cells, high efficiency operation at a temperature of 300 °C has been demonstrated,[29–32] which is superior to traditional Si or III-V solar cells. Despite the promising results, very few studies on the thermal reliability of InGaN solar cells exist, and their degradation mechanisms at high temperature are still unclear. In addition to crystal qualities, other device parameters such as metal contacts, passivation layers, and surface properties of the solar cell will also play significant roles in determining the thermal reliability of devices at high temperatures. For example, a recent study has shown that the semiconductor/metal interface of p–GaN/Ni/Au contacts is particularly vulnerable to Ni diffusion in GaN layers at high temperature and eventually cracks after 700 °C thermal treatment.[26] This will lead to degraded contact performance in InGaN solar cells at high temperatures. In contrast, n–GaN/metal contacts, typically formed in Ti/Al bilayers, were found to be thermally stable, possibly due to intermetallic compounds and high annealing temperatures.[25,33,34]

In this paper, we perform comprehensive studies on the thermal stability of InGaN multi-quantum-well (MQW) solar cells under thermal stress at 400 °C, 450 °C, and 500 °C. Both *ex situ* electrical measurements and material characterization were performed to analyze the possible degradation mechanisms of InGaN solar cells under high temperature conditions. After thermal stress testing, the external quantum efficiency (EQE) spectra of the devices showed a small degree of degradation, while the short-circuit current (J_{sc}) remained nearly constant for all samples. The reduction of energy conversion efficiency was mainly attributed to the drop of open-circuit voltage (V_{oc}), possibly due to the degraded contact performance under thermal stress. Furthermore, by fitting the Arrhenius equation, the failure lifetime of the InGaN solar cells at different temperatures was also obtained. These results suggest that while InGaN solar cells have high thermal stability, the degradation in the metal contact could be the major

a)Yuji.Zhao@asu.edu

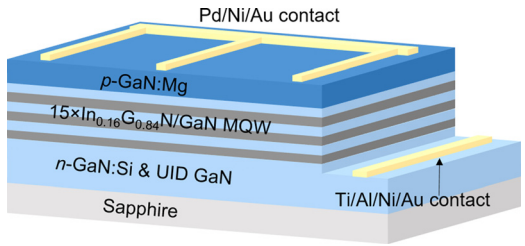

FIG. 1. The schematic structure of InGaN MQW solar cell samples investigated in the thermal stress testing.

limiting factor for these devices under high temperature operation.

The InGaN MQW solar cell epi-structures were grown by conventional metal-organic chemical vapor deposition (MOCVD) on (0001) sapphire. The indium incorporation was determined to be 16% using photoluminescence measurements and was further verified using High Resolution X-Ray Diffraction (HRXRD) measurements. The device structure consists of 2 μm Si-doped n–GaN ([Si]=3×10^{18} cm^{-3}), 125 nm highly Si-doped n$^+$–GaN ([Si] = 2×10^{19} cm^{-3}), 15 periods of InGaN (3 nm)/GaN (6.6 nm) MQWs, 110 nm Mg-doped p–GaN, and 10 nm highly Mg-doped p$^+$–GaN contact layers. The InGaN epi-structures were processed into solar cell devices with 1 mm × 1 mm mesas using standard contact lithography and inductively coupled plasma (ICP) etching. Ti/Al/Ni/Au ring contacts and Pd/Ni/Au grid contacts were deposited around the perimeter and on the top of the mesas, respectively. Both contacts were deposited via electron beam evaporation and then annealed at 500 °C in a N_2 atmosphere for 5 min using a rapid-thermal annealing process. None of the solar cell devices were coated with ITO or current spreading layers. The schematic structure of the InGaN MQW solar cells is shown in Fig. 1.

The crystal qualities of the InGaN MQW solar cell samples before and after the thermal stress treatment were characterized by the High Resolution X-Ray Diffraction (HRXRD) measurement using a PANalytical X'Pert Pro materials research X–ray diffractometer (MRD) system with Cu Kα radiations. A hybrid monochromator and a triple axis module were used for the incident and diffracted beam optics, respectively. Illuminated *J–V* measurements were taken using an Oriel Class A Solar Simulator at the 1 sun condition under the AM1.5D spectrum. EQE measurement data were collected using an Oriel QEPVSI quantum efficiency measurement system and calibrated with a reference Si photodetector. More details on *J–V* and EQE measurements can be found in Refs. 11 and 35. For thermal stress testing, the InGaN solar cell devices were subject to 400 °C, 450 °C, and 500 °C in a N_2 atmosphere using a Minibrute furnace. The time duration for each thermal stress period was set to be 2 h. The devices were taken out from the furnace and cooled down to room temperature for *ex situ* electrical and material characterization. After all measurements, the devices were placed back in the furnace for another 2-h period of thermal stress. The total time for the thermal treatment is 8 h.

Before device characterization, the HRXRD measurement was performed to analyze the material quality of the samples. (002) symmetric and (102) asymmetric plane rocking curves (RCs) were measured before and after each period of thermal stress. The obtained full-width-half-maximum (FWHM) values from (002) and (102) plane RCs are shown in Figs. 2(a) and 2(b). The screw and edge dislocation densities were also calculated based on the following equation:[36]

$$\rho = \frac{\beta^2}{4.35\vec{b}^2}, \tag{1}$$

where ρ is the dislocation density, β is the FWHM value, and $\vec{b}$ is the Burgers vector. For samples under 400 °C and 450 °C stress, considering the variation from instrumental and measurement factors, FWHM values of (002) and (102) RCs are nearly constant with variations within 5%. The largest and smallest FWHM values of (002) RCs are 247 arc sec and 235 arc sec at 400 °C and 240 arc sec and 231 arc sec at 450 °C, respectively. For (102) RCs, those values range from 272 arc sec to 265 arc sec at 400 °C and from 267 arc sec to 251 arc sec at 450 °C. These results indicate that material quality remains nearly unchanged throughout the thermal stress testing. Furthermore, for samples under 500 °C stress testing, it was observed that the FWHM values decrease considerably [−13% for (002) and −9% for (102) RCs]. These reduced FWHM values suggest that the dislocation density in the samples reduced as thermal stress testing proceeded. This improvement of material quality can be attributed to the quenching effect on the epitaxial layers. This effect has also been observed in other studies, where InGaN solar cell samples had been annealed at 450 °C or higher temperatures and QW re-homogenization was observed in the transmission-electron-microscopy study.[37,38] These results show that moderate thermal stress (e.g., 400–500 °C) will have a minimum negative impact on the material quality of InGaN solar cells. This is also consistent with the fact that III-N materials are typically epitaxially grown at extremely high temperature (e.g., ~1000 °C) and therefore should be robust under high temperature stress.

Figure 3 shows the time evolution of the representative EQE spectra of InGaN samples under (a) 400 °C, (b) 450 °C, and (c) 500 °C thermal stress testing. Overall, all the samples

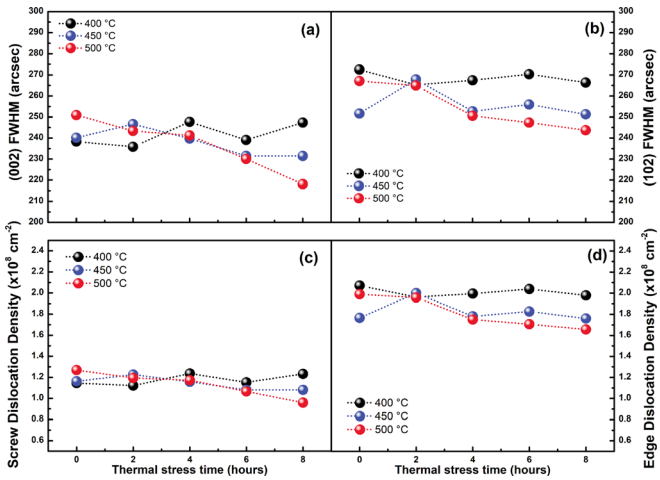

FIG. 2. The obtained full-width-half-maximum (FWHM) values from (a) (002) and (b) (102) plane RCs for InGaN solar cell samples. The calculated screw and edge dislocation densities are shown in (c) and (d), respectively.

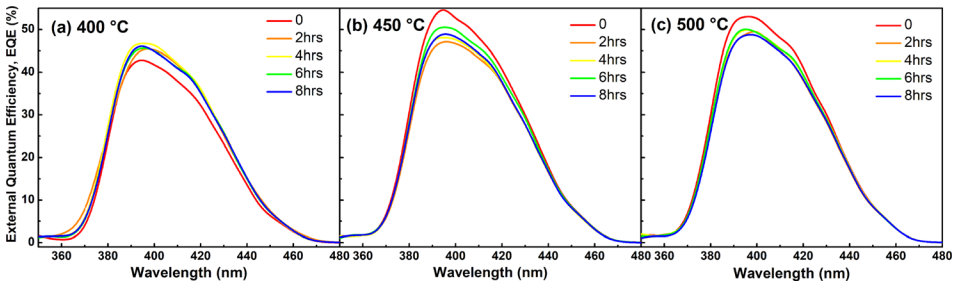

FIG. 3. The time evolution of the representative EQE spectra of the InGaN solar cell samples under (a) 400 °C, (b) 450 °C, and (c) 500 °C thermal stress testing.

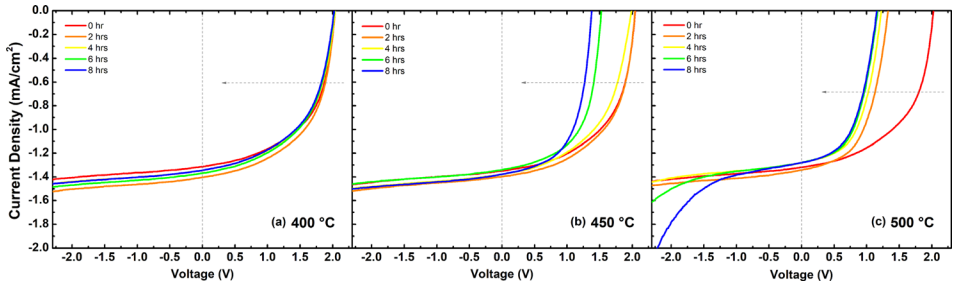

FIG. 4. The illuminated current density–voltage (*J*–*V*) curves as functions of stress time for 3 InGaN solar cell devices under (a) 400 °C, (b) 450 °C, and (c) 500 °C thermal stress testing.

exhibit robust thermal reliability in terms of EQE performance. With the increasing stress time, EQEs in the short and long wavelength regimes are almost constant at all temperatures, while small variations around the peak EQE regions were observed possibly due to the variation of measurements from the setup. The robust EQE performance stems from the robustness of III-N materials. This also corresponds to the nearly steady values of J_{sc}, which will be discussed in detail later.

Figure 4 presents the illuminated current density–voltage (*J*–*V*) measurements of devices as a function of stress time for InGaN solar cells under (a) 400 °C, (b) 450 °C, and (c) 500 °C thermal stress. Figure 5 shows the obtained values of (a) V_{oc}, (b) J_{sc}, (c) fill factor (FF), and (d) energy conversion efficiency from the *J*–*V* curves in Figs. 4(a)–4(c). Both J_{sc} and FF showed a minimal variation with the increasing stress time at all temperatures. The trends of J_{sc} values are also in good agreement with the EQE spectra, which shows strong resistance to thermal stress. At 400 °C stress, minimum degradation is observed in V_{oc} and the efficiency remains almost constant around 1.4%. While at 450 °C stress, V_{oc} reduces gradually from 2.05 V (0 h) to 1.99 V (4 h) and then 1.38 V (8 h) as stress time increases. The conversion efficiency of the solar cell is the product of V_{oc}, J_{sc}, and FF. Since J_{sc} and FF are almost constant in this study, the conversion efficiency is predominately determined by V_{oc} of the InGaN solar cells. Therefore, the efficiency reduces from 1.52% (0 h) to 1.42% (4 h) and then to 1.10% (8 h). At 500 °C, V_{oc} degrades more severely, which ranges from 2.03 V (0 h) to 1.22 V (4 h) and then 1.15 V (8 h). Accordingly, the efficiency of the solar cells drops from 1.42% (0 h) to 0.84% (4 h) and then to 0.76% (8 h). In addition, the leakage current at negative bias for the InGaN solar cells increases dramatically, as shown in Fig. 4(c), which indicates a strong degradation in junction behavior. From the above results, the reduction in V_{oc} appears to be the major degradation mechanism in InGaN solar cells under the thermal stress. Since the thermal stress had minimum impacts on the material quality of the InGaN solar cell samples (as shown in previous HRXRD studies), we performed comprehensive electrical characterization on the metal contacts of the InGaN solar cells under thermal stress. The electrical properties of N-type metal contacts were also measured, and minimum degradation was observed (data not shown here).

The electrical behavior of the p-GaN/metal contact was investigated by the transmission line method (TLM) at room temperature (RT) after samples were taken out of the furnace. Figure 6 presents the time evolution of I–V characteristics of the p-GaN/Pd/Ni/Au contacts (20 μm TLM) of the InGaN solar cell devices under (a) 400 °C, (b) 450 °C, and (c) 500 °C thermal stress testing. For samples under 400 °C stress testing, the contact was affected to a certain extent but still maintained a "semi-ohmic" behavior. At 0.5 V bias, the current drops from 2.76×10^{-5} A (0 h) to 2.10×10^{-5} A (4 h) and then to 1.86×10^{-5} A (8 h). However, for those solar cells under 450 °C and 500 °C stress testing, the contact behavior changes dramatically from ideal ohmic to the rectifying Schottky behavior. Moreover, the sample under 500 °C stress experienced much more severe degradation than the

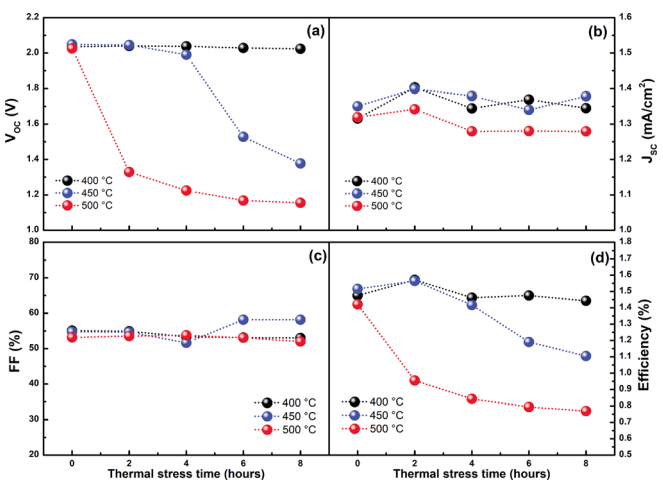

FIG. 5. The obtained values of (a) open-circuit voltage (V_{oc}), (b) short-circuit current (J_{sc}), (c) fill factor (FF), and (d) energy conversion efficiency for the InGaN solar cells from *J*–*V* curves in Figs. 4(a)–4(c).

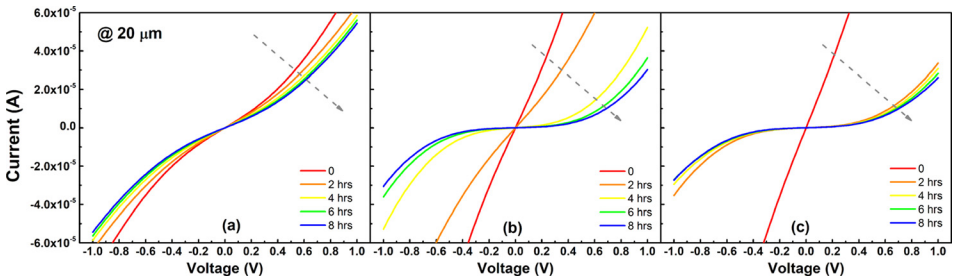

FIG. 6. The time evolution of I–V characteristics of the p-GaN/Pd/Ni/Au contacts (20 μm TLM) for 3 InGaN solar cell samples under (a) 400 °C, (b) 450 °C, and (c) 500 °C thermal stress testing.

one under 450 °C stress. Theoretically, V_{oc} of a solar cell can be determined from the diode equation as[39]

$$V_{OC} = \frac{nkT}{q}\ln\left(\frac{J_{SC}}{J_0} + 1\right), \tag{2}$$

$$J_0 = J_{0,bulk} + J_{0,contact} = J_{0,bulk} + qS_{eff}(\Delta p + \Delta n), \tag{3}$$

where n is the ideality factor, T is the temperature, k is Boltzmann's constant, q is the electron charge, J_0 is the dark saturation current density, S_{eff} is the effective surface recombination velocity, and Δp and Δn are the excess minority carrier concentrations near the contact interface. As contact properties are compromised, a large amount of defect states near the contact/p-GaN interface after thermal stress were generated. These defects or trap states result in the increase in the surface recombination current, which leads to the rising $J_{0,contact}$ and thus the reduced V_{oc}. The schematic band diagram of the metal/p-GaN contact of InGaN MQW solar cell samples after the thermal stress testing is shown in Fig. S1 in the supplementary material. Furthermore, Fig. S2 (supplementary material) shows the scanning electron microscopy (SEM) images of p-type metal contacts before and after thermal stress. It can be observed that the surface morphologies of the metal contacts became rougher after the thermal stress. Bubbles and cracks on metal contacts were observed in the sample after 500 °C thermal stress. This contact morphology degradation after thermal stress is also consistent with previous studies.[33,40] The compromised contact behavior is therefore likely to contribute to the reduction in V_{oc} and efficiency of the solar cell devices.

Dark J–V measurements were further performed to analyze the electrical properties of InGaN solar cell samples after thermal stress testing. Based on the following equation:[39]

$$\frac{dV}{dJ} = R_S + \frac{nkT}{q}(J + J_{SC})^{-1}, \tag{4}$$

the series resistances (R_s) and ideality factor n of the devices were obtained from the intercepts of the linear fitting results for plots of $\frac{dV}{dJ}$ vs $(J + J_{SC})^{-1}$, which are presented in Fig. 7. The inset tables show the obtained values of R_s and n. The large ideality factor n over 2 can be caused by several mechanisms such as tunneling effects, leakage currents, and defect-related generation and recombination at the contacts and/or in the bulk of devices.[41,42] All devices exhibited increased n after thermal stress. One possible reason may be more leakage paths generated during the process of thermal stress. Another reason can be related to the degraded contact behaviors after thermal stress as shown in Fig. 5. Furthermore, the InGaN solar cell under 500 °C stress showed the largest increase in n values. This is consistent with the large leakage current observed in Fig. 4(c).

The Arrhenius model was employed to predict the failure lifetime (t_f) of InGaN solar cell samples, which is a standard approach for the microelectronic reliability study.[43,44] It is often presented as the following equation: $t_f = Ae^{\frac{E_a}{kT}}$, where A is a scaling factor and E_a is the activation energy (eV) for the specific failure mechanism at temperature T. It can be further derived as $\ln t_f = E_a \cdot \frac{1}{kT} + \ln A$. The assumption here is that the degradation mechanisms are the same in the range of 400 °C–500 °C. By linearly fitting the plots of efficiency vs. stress time and defining t_f as the value when efficiency drops to 1/3 of its initial value, we can obtain t_f values for the solar cell samples, which are 133.8, 19.1, and 11.2 h, respectively. The activation energy, $E_a = 1.124$ eV, and the scaling factor, $A = 4.244 \times 10^{-7} h$, can be obtained via fitting the Arrhenius plot in Fig. 8(b). Therefore, the estimated lifetimes for InGaN solar cells are 3244 h at 300 °C, 523 h at 350 °C, and 55 h at 425 °C. Note that passivation layers were not coated in our devices. The estimated lifetime will thus be expected to be greatly improved if they are included.

In conclusion, we studied the thermal stability of InGaN solar cells by employing thermal stress testing in N_2 at 3 different temperatures: 400 °C, 450 °C, and 500 °C. The stable EQE characteristics reveal the thermal robustness of InGaN solar cells. Analysis of J–V curves shows that the reduction of V_{oc} is mainly responsible for the degradation of efficiency after thermal stress, where J_{sc} and FF are almost constant. Furthermore, the results from TLM and HRXRD measurements suggest that the deteriorated contacts under thermal stress may be the major degradation mechanisms for InGaN solar cells, while the crystal quality of InGaN had minimum

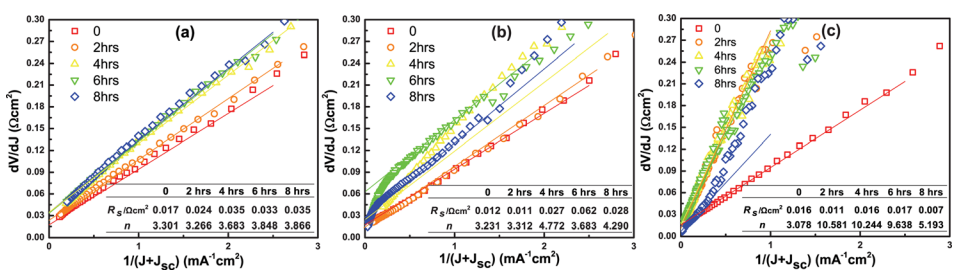

FIG. 7. Plots of $\frac{dV}{dJ}$ vs $(J + J_{SC})^{-1}$ and the linear fit curves for the InGaN solar cell devices. The inset tables show the obtained series resistance (R_s) and ideality factor n.

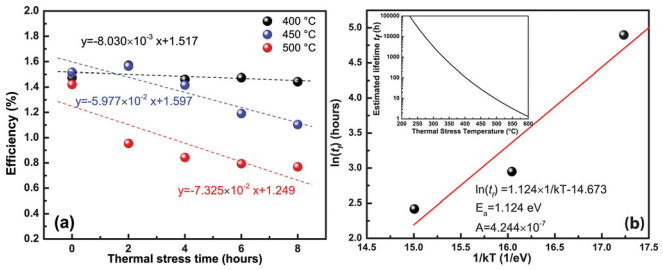

FIG. 8. (a) Energy conversion efficiency as a function of stress time for the InGaN solar cell devices under 400 °C, 450 °C, and 500 °C thermal stress testing and their corresponding linear fittings. (b) Arrhenius plot of $\ln t_f$ vs $\frac{1}{kT}$ for the InGaN solar cells. The inset shows the estimated failure lifetime at different temperatures.

negative impacts from the thermal stress. Additionally, we also estimated the failure lifetime of InGaN solar cells at different temperatures by fitting the Arrhenius model. Our results show that InGaN solar cells are capable of maintaining PV performance at high temperature, and special attention has to be paid towards the design and fabrication of the metal contact of InGaN solar cells for high temperature operations.

See supplementary material for the SEM images of p-contact metals of InGaN MQW solar cell samples before and after thermal stress (Fig. S1) and the schematic band diagram of the metal/p-GaN contact of InGaN MQW solar cell samples after the thermal stress testing (Fig. S2).

This work was supported by an Early Career Faculty grant from NASA's Space Technology Research Grants Program. The authors would like to express sincere gratitude to Professor Yong-Hang Zhang at Arizona State University for access to his optoelectronics characterization laboratory. The authors would also like to thank Mr. Jia Ding for the help in IV and EQE measurements. We gratefully acknowledge the use of facilities within the LeRoy Eyring Center for Solid State Science at Arizona State University.

[1]Y.-F. Wu, D. Kapolnek, J. P. Ibbetson, P. Parikh, B. P. Keller, and U. K. Mishra, IEEE Trans. Electron Devices **48**, 586 (2001).
[2]H. Fu, X. Huang, H. Chen, Z. Lu, X. Zhang, and Y. Zhao, IEEE Electron Device Lett. **38**, 763 (2017).
[3]D. Disney, H. Nie, A. Edwards, D. Bour, H. Shah, and I. C. Kizilyalli, in *2013 25th International Symposium on Power Semiconductor Devices ICs*, ISPSD (2013), pp. 59–62.
[4]H. Fu, I. Baranowski, X. Huang, H. Chen, Z. Lu, J. Montes, X. Zhang, and Y. Zhao, IEEE Electron Device Lett. **38**, 1286 (2017).
[5]Y. Zhao, S. Tanaka, C.-C. Pan, K. Fujito, D. Feezell, J. S. Speck, S. P. DenBaars, and S. Nakamura, Appl. Phys. Express **4**, 082104 (2011).
[6]H. Chen, H. Fu, X. Huang, Z. Lu, X. Zhang, J. Montes, and Y. Zhao, IEEE Photonics J. **9**, 8200808 (2017).
[7]H. Chen, H. Fu, Z. Lu, X. Huang, and Y. Zhao, Opt. Express **24**, A856 (2016).
[8]O. Jani, I. Ferguson, C. Honsberg, and S. Kurtz, Appl. Phys. Lett. **91**, 132117 (2007).
[9]X. Huang, H. Fu, H. Chen, Z. Lu, D. Ding, and Y. Zhao, J. Appl. Phys. **119**, 213101 (2016).
[10]A. G. Bhuiyan, K. Sugita, A. Hashimoto, and A. Yamamoto, IEEE J. Photovoltics **2**, 276 (2012).
[11]X. Huang, H. Fu, H. Chen, X. Zhang, Z. Lu, J. Montes, M. Iza, S. P. DenBaars, S. Nakamura, and Y. Zhao, Appl. Phys. Lett. **110**, 161105 (2017).
[12]H. Fu, Z. Lu, X. Huang, H. Chen, and Y. Zhao, J. Appl. Phys. **119**, 174502 (2016).
[13]M. Hou, H. So, A. J. Suria, A. S. Yalamarthy, and D. G. Senesky, IEEE Electron Device Lett. **38**, 56 (2017).
[14]H. Fu, H. Chen, X. Huang, Z. Lu, and Y. Zhao, J. Appl. Phys. **121**, 014501 (2017).
[15]Z. Lu, P. Tian, H. Chen, I. Baranowski, H. Fu, X. Huang, J. Montes, Y. Fan, H. Wang, X. Liu, R. Liu, and Y. Zhao, Opt. Express **25**, 17971 (2017).
[16]J. Wu, J. Appl. Phys. **106**, 011101 (2009).
[17]J. Wu, W. Walukiewicz, K. M. Yu, W. Shan, J. W. A. Iii, E. E. Haller, H. Lu, W. J. Schaff, W. K. Metzger, and S. Kurtz, J. Appl. Phys. **94**, 6477 (2003).
[18]H. M. Branz, W. Regan, K. J. Gerst, J. B. Borak, and E. A. Santori, Energy Environ. Sci. **8**, 3083 (2015).
[19]R. Dahal, J. Li, K. Aryal, J. Y. Lin, and H. X. Jiang, Appl. Phys. Lett. **97**, 073115 (2010).
[20]C. J. Ercol, J. Jenkins, G. Dakermanji, A. G. Santo, and L. S. Mason, in *Collection of Technical Papers 35th Intersociety Energy Conversion Engineering Conference Exhibit*, IECEC Catalogue No. 00CH37022 (2000), Vol. 1, pp. 449–459.
[21]G. A. Landis, D. Merritt, R. P. Raffaelle, and D. Scheiman, in *Proceedings 18th Space Photovoltaic Res. Technol. Conf.* (2005), pp. 241–247.
[22]A. J. Suria, A. S. Yalamarthy, T. A. Heuser, A. Bruefach, C. A. Chapin, H. So, and D. G. Senesky, Appl. Phys. Lett. **110**, 253505 (2017).
[23]F. Medjdoub, J. F. Carlin, C. Gaquière, N. Grandjean, and E. Kohn, Open Electr. Electron. Eng. J. **2**, 1 (2008).
[24]P. G. Neudeck, R. S. Okojie, and L.-Y. Chen, Proc. IEEE **90**, 1065 (2002).
[25]M. Hou and D. G. Senesky, Appl. Phys. Lett. **105**, 081905 (2014).
[26]S. Zhao, H. McFavilen, S. Wang, F. A. Ponce, C. Arena, S. Goodnick, and S. Chowdhury, J. Electron. Mater. **45**, 2087 (2016).
[27]D. Maier, M. Alomari, N. Grandjean, J. F. Carlin, M. A. Diforte-Poisson, C. Dua, A. Chuvilin, D. Troadec, C. Gaquiere, U. Kaiser, S. L. Delage, and E. Kohn, IEEE Trans. Device Mater. Reliab. **10**, 427 (2010).
[28]D. Maier, M. Alomari, N. Grandjean, J. F. Carlin, M. A. Diforte-Poisson, C. Dua, S. Delage, and E. Kohn, IEEE Electron Device Lett. **33**, 985 (2012).
[29]L. Zhao, T. Detchprohm, and C. Wetzel, Appl. Phys. Lett. **105**, 243903 (2014).
[30]D.-H. Lien, Y.-H. Hsiao, S.-G. Yang, M.-L. Tsai, T.-C. Wei, S.-C. Lee, and J.-H. He, Nano Energy **11**, 104 (2015).
[31]J. J. Williams, H. McFavilen, A. M. Fischer, D. Ding, S. R. Young, E. Vadiee, F. A. Ponce, C. Arena, C. B. Honsberg, and S. M. Goodnick, *In 2016 IEEE 43rd Photovoltaic Specialists Conference, PVSC* (2016), pp. 0193–0195.
[32]Y. Zhao, X. Huang, H. Fu, H. Chen, Z. Lu, J. Montes, and I. Baranowski, in *2017 IEEE 60th International Midwest Symposium Circuits and Systems*, MWSCAS (2017), pp. 954–957.
[33]F. Iucolano, F. Roccaforte, A. Alberti, C. Bongiorno, S. Di Franco, and V. Raineri, J. Appl. Phys. **100**, 123706 (2006).
[34]F. Lin, B. Shen, S. Huang, F. J. Xu, L. Lu, J. Song, F. H. Mei, N. Ma, Z. X. Qin, and G. Y. Zhang, J. Appl. Phys. **105**, 093702 (2009).
[35]Y. Zhao, M. Boccard, S. Liu, J. Becker, X.-H. Zhao, C. M. Campbell, E. Suarez, M. B. Lassise, Z. Holman, and Y.-H. Zhang, Nat. Energy **1**(6), 16067 (2016).
[36]J. C. Zhang, D. G. Zhao, J. F. Wang, Y. T. Wang, J. Chen, J. P. Liu, and H. Yang, J. Cryst. Growth **268**, 24 (2004).
[37]E. Vadiee, J. J. Williams, S. Zhao, C. Hongsberg, S. Goodnick, E. Clinton, C. Fabien, and A. Doolittile, in 59th Electronic Materials Conference, EMC (2017).
[38]N. A. K. Kaufmann, A. Dussaigne, D. Martin, P. Valvin, T. Guillet, B. Gil, F. Ivaldi, S. Kret, and N. Grandjean, Semicond. Sci. Technol. **27**, 105023 (2012).
[39]S. S. Hegedus and W. N. Shafarman, Prog. Photovoltics Res. Appl. **12**, 155 (2004).
[40]A. J. Suria, A. S. Yalamarthy, H. So, and D. G. Senesky, Semicond. Sci. Technol. **31**, 115017 (2016).
[41]F. Ren, A. P. Zhang, G. T. Dang, X. A. Cao, H. Cho, S. J. Pearton, J.-I. Chyi, C.-M. Lee, and C.-C. Chuo, Solid-State Electron. **44**, 619 (2000).
[42]H. Fu, X. Huang, H. Chen, Z. Lu, and Y. Zhao, IEEE J. Electron Devices Soc. **5**, 518 (2017).
[43]M. Omori, J. N. Wholey, and J. F. Gibbons, in *18th International Reliability Physics Symposium* (1980), pp. 134–139.
[44]E. B. Hakim, Qual. Reliab. Eng. Int. **7**, 215 (1991).